

# Instabilities of the flow in a curved channel with compliant walls

BY ANAÏS GUAUS<sup>†</sup> AND ALESSANDRO BOTTARO\*

*DICAT, Università di Genova, Via Montallegro 1, 16145 Genova, Italy*

The linear stability of flows in curved compliant channels is examined. The walls bounding the fluid are modelled as thin cylindrical shells supported by a rigid outer frame through arrays of springs and dampers; this is often referred to as Kramer-type coating. Sufficiently soft compliant walls have an influence on the large-scale streamwise vortices produced in the channel by the centrifugal force, although the effect is limited to modes of large enough spanwise wavelengths. For even longer wavelengths, a spanwise-periodic surface-based wave precedes the onset of the streamwise vortex instability. Longitudinal or oblique travelling-wave flutter modes may appear and dominate the transition scenario, for sufficiently compliant walls, depending on the receptivity conditions.

**Keywords:** hydrodynamic stability; flow-induced surface instabilities; compliant walls; curved channel flow; Dean vortices

## 1. Introduction

The idea of tailoring the characteristics of solid walls to control the fluid flowing over them originates from Gray (1936)'s observations of swimming dolphins and from the assumption that their high propulsive efficiency should be ascribed to the compliance of their skins. Many studies followed including in particular the tests by Kramer (1957, 1960), which appeared to demonstrate the efficiency of compliant surfaces in delaying transition to turbulence. Given the importance of the subject for its implications on control and manoeuvring of aerial and marine vehicles, many people approached the problem from the theoretical point of view to shed light on the interactions between the fluid and the solid. Initial theories were laid out by Benjamin (1960) and Landahl (1962), who focused on the behaviour of small disturbances in the system, after modelling the solid as a thin elastic membrane. In the approach by Carpenter and co-workers (Carpenter & Garrad 1985, 1986; Carpenter 1990; Davies & Carpenter 1997*a,b*; Carpenter *et al.* 2000), a surface-based compliant wall model is adopted; a thin plate is supported by a rigid foundation through springs and dampers. A more realistic approach consists in the use of volume-based methods that start from the continuum equations of solid mechanics and cater naturally to anisotropic multilayered materials. The efforts of Yeo and co-workers are notable in this respect (Yeo & Dowling 1987; Yeo 1988, 1990, 1992, 1994; Yeo *et al.* 1994, 2001).

\* Author for correspondence (alessandro.bottaro@unige.it).

<sup>†</sup> Present address: IMFT, Allée du Pr. C. Soula, 31400 Toulouse, France.

On the other hand, the simplicity of surface-based models appealed to many other researchers (Denier & Hall 1991; Nagata & Cole 1999; Wiplier & Ehrenstein 2001; Allen & Bridges 2003; Davies 2003; Xu *et al.* 2003) allowing them to make rapid progress in the understanding of the transition-delaying potential of different types of wall coatings in a variety of configurations.

The problem addressed here aims at elucidating the effect of wall compliance on the instabilities developing in a curved channel. It has been known for approximately 80 years that curvature sustains the amplification of longitudinal vortices in channels (Dean 1928), and longitudinal or quasi-longitudinal vortices arise in a variety of technological applications that involve curved passages and ducts, affecting strongly heat transfer coefficients and friction factors. However, the interactions that take place when the bounding walls are not infinitely rigid are unknown. Limited experimental evidence has been produced for the case in which the vortices are present in a boundary layer next to a curved compliant wall. Yurchenko & Babenko (1987) observed that a porous rubber coating could delay the amplification of Görtler vortices developing over the concave wall of a water channel. A very mild stabilizing effect is found when the large Görtler number and spanwise wavenumber limits are taken (Denier & Hall 1991), but the theory does not address the behaviour of flow-induced surface waves. It will be shown here that such hydroelastic waves, related to the compliance of the bounding walls, are important and could trigger early transition.

Before providing a brief overview of the different kinds of flow-induced surface modes, we wish to briefly comment on the expected effect of flexible walls on hydrodynamic waves. Surface compliance acts primarily in a near-wall viscous layer; the Dean instability originates from an inviscid mechanism, related to the curvature of the flow streamlines, and the vortices occupy the whole cross-section of the curved channel. On first impression, thus, it might be expected that compliant coating should have but a mild effect on Dean vortices. On the other hand, also crossflow vortices such as those arising in the boundary layer on a rotating disc are inviscidly unstable, but compliant coating can strongly stabilize them (Cooper & Carpenter 1997*a,b*; Davies & Carpenter 2001, 2003). It is thus not so immediate to anticipate on the effect of wall coating on the steady Dean modes. In the case of viscous (Tollmien–Schlichting) instabilities, wall compliance acts by modifying the phase relationship between the streamwise and the wall-normal perturbation velocity components, thus changing the Reynolds stress and consequently the energy balance. Criteria for the complete suppression of Tollmien–Schlichting waves have been given, but, if the wall is too compliant, the effect on transition to turbulence can be opposite to the expected one, owing to the premature appearance of hydroelastic modes. In the present configuration, Tollmien–Schlichting modes should not hold a role, given the exceedingly small value of the curvature parameter needed for them to appear before the Dean vortices, at any value of the Reynolds number.

Just as in the case of the rotating disk boundary layer (Cooper & Carpenter 1997*a*), wall compliance greatly increases the complexity of the eigenmodes' spectrum. A sketch of the geometry under consideration, with some of the modes which can appear, is provided in figure 1. The most important flow-induced surface instabilities (FISI) are travelling-wave flutter (TWF) and static divergence (SD). They are the incompressible analogue of classical aeroelastic phenomena: flutter and divergence. Flutter of thin panels consists of the

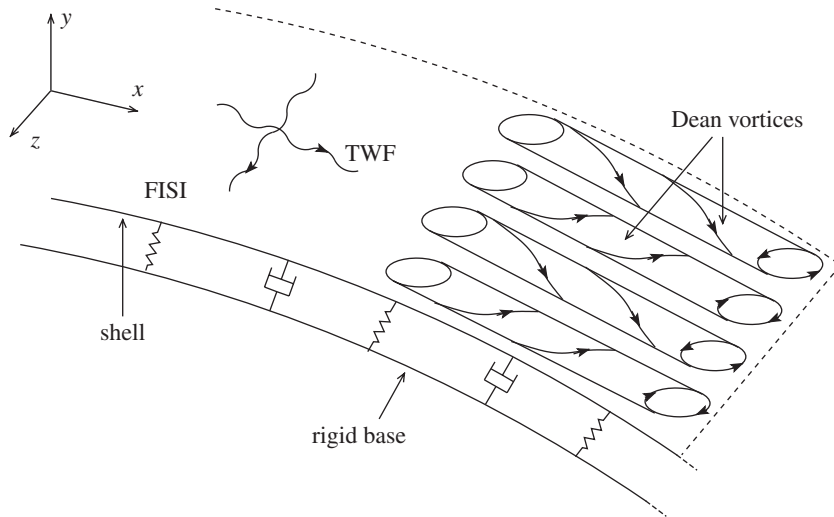


Figure 1. Sketch of the problem under investigation with some of the instability modes which can emerge: Dean vortices, TWF and spanwise-periodic surface waves (simply labelled as FIS). The upper wall is not shown. Both walls are modelled as thin elastic shells supported by rigid frames through arrays of springs and dampers.

self-excited oscillations of plates and/or shells exposed on one side to a, usually transonic or supersonic, stream of air; the prevention of flutter modes represents a primary design criterion for aerospace structures. Divergence occurs when a lifting surface deflects under aerodynamic load so that the applied load is either increased or displaced so as to enhance the twisting effect on the structure.

In the incompressible setting, TWF has been usually identified as a high-frequency streamwise travelling wave, capable of leading to rapid breakdown to turbulence when a critical flow speed, which increases with the wall stiffness, is exceeded. [Davies & Carpenter \(1997a\)](#) report that the fluid layers nearest to the walls play a crucial role in stabilizing TWF, and the stabilization is enhanced by wall damping, i.e. when a viscous fluid substrate or viscoelastic losses are included in the wall model. In the present paper, TWF modes are computed and a previously unreported standing or travelling FIS is discovered.

Static divergence occurs in the form of very slowly travelling or stationary waves of long wavelength and, as such, can have an effect similar to that of surface roughness. Its characteristics have often been difficult to determine: it is associated with the onset of an absolute instability and its occurrence is reportedly dominated by the presence of nonlinear effects ([Gad-el-Hak 1986, 2000](#)). As shown by [Landahl \(1962\)](#), SD can be qualitatively described using potential flow theory (TWF cannot) and wall damping is necessary for its appearance. According to [Davies & Carpenter \(1997a\)](#), SD is unlikely to appear when coatings that are efficient at stabilizing Tollmien–Schlichting waves are considered; it arises when the flow moves at a speed much larger than the elastic shear-wave speed of the material so that the internal restoring forces in the walls (related to the coating stiffness) are outweighed by the large disturbance pressure imposed by the fluid. When this happens, a unidirectional transfer of energy towards the solid occurs.

It should be noted that other forms of FISI characterized by coalescing modes have been reported in the literature, with strong interactions possible between TWF modes and either divergence or Tollmien–Schlichting waves, possibly leading to absolute instabilities. With the parameters adopted in this research, we have neither observed coalescing modes nor SD waves.

This brief overview makes clear that this hydroelastic problem is very rich and that a large number of parameters must be accounted for (curvature, Reynolds number, coating parameters such as flexural rigidity, elasticity, damping properties, etc.). For the sake of clarity, after a description of the stability equations and of the surface-based wall equations adopted, we have divided the instability modes into three classes and dedicated a section to each class: two-dimensional streamwise homogeneous (Dean-like) modes; two-dimensional spanwise homogeneous (Tollmien–Schlichting-like) modes; and three-dimensional modes. A summary of the findings and concluding remarks are left for the last section of the paper.

## 2. The model

We consider the flow of an incompressible, Newtonian fluid in a slightly curved channel bounded by two compliant walls. When undeformed, the walls are separated by a distance  $2h$ ; the constant radius of curvature at the channel centreline is  $R$ , and the curvature parameter defined as  $\gamma = 2h/R$ , is taken to be small, in such a way that, to first order in  $\gamma$ , the dimensionless base flow reads (Matsson & Alfredsson 1990)

$$U = (1 - y^2) \left( 1 - \frac{1}{3} \gamma y \right). \quad (2.1)$$

In this expression, the velocity has been scaled with the centreline velocity  $U_0$  and  $y$  is the dimensionless normal-to-the-wall coordinates defined below.

### (a) Linear stability equations

The Navier–Stokes equations in cylindrical coordinates  $(r, \theta, \xi)$  written for the primitive variables  $(u_r, u_\theta, u_\xi, p^*)$  are linearized about a mean flow  $U_\theta(r)$ . Since the curvature parameter  $\gamma$  is small, it is convenient to define a set of ‘pseudo-Cartesian’ coordinates  $(x, y, z)$  representing the streamwise direction, the direction normal to the wall and the spanwise direction, respectively. Such coordinates in dimensionless form are

$$x = \frac{2\theta}{\gamma}, \quad y = \frac{2(r-R)}{\gamma R}, \quad z = \frac{2\xi}{\gamma R}. \quad (2.2)$$

The new dependent variables  $(u, v, w, p)$  and time  $t$  are obtained after scaling the dimensional variables as follows:

$$u = \frac{u_\theta}{U_0}, \quad v = \frac{u_r}{U_0}, \quad w = \frac{u_\xi}{U_0}, \quad p = \frac{p^*}{\rho U_0^2}, \quad t = \frac{U_0}{h} t^*. \quad (2.3)$$

To first order in  $\gamma$ , the linearized equations of motion are

$$\left\{ \begin{aligned} \frac{\partial u}{\partial x} + \frac{\partial v}{\partial y} + \frac{\partial w}{\partial z} + \frac{\gamma}{2}v - \frac{\gamma}{2}y \frac{\partial u}{\partial x} &= 0, \\ \frac{\partial u}{\partial t} + \left(1 - \frac{\gamma y}{2}\right) U \frac{\partial u}{\partial x} + U'v + \frac{\gamma}{2}Uv &= -\left(1 - \frac{\gamma y}{2}\right) \frac{\partial p}{\partial x} + \frac{1}{Re} \Delta u \\ &+ \frac{\gamma}{Re} \left( \frac{1}{2} \frac{\partial u}{\partial y} - y \frac{\partial^2 u}{\partial x^2} + \frac{\partial v}{\partial x} \right), \\ \frac{\partial v}{\partial t} + \left(1 - \frac{\gamma y}{2}\right) U \frac{\partial v}{\partial x} - \gamma Uu &= -\frac{\partial p}{\partial y} + \frac{1}{Re} \Delta v + \frac{\gamma}{Re} \left( \frac{1}{2} \frac{\partial v}{\partial y} - y \frac{\partial^2 v}{\partial x^2} - \frac{\partial u}{\partial x} \right), \\ \frac{\partial w}{\partial t} + \left(1 - \frac{\gamma y}{2}\right) U \frac{\partial w}{\partial x} &= -\frac{\partial p}{\partial z} + \frac{1}{Re} \Delta w + \frac{\gamma}{Re} \left( \frac{1}{2} \frac{\partial w}{\partial y} - y \frac{\partial^2 w}{\partial x^2} \right), \end{aligned} \right. \quad (2.4)$$

where  $Re = U_0 h / \nu$  is the Reynolds number and  $\Delta$  is the operator  $(\partial^2/\partial x^2) + (\partial^2/\partial y^2) + (\partial^2/\partial z^2)$ . Strictly speaking, the equations above are not  $O(1)$  in  $\gamma$  since terms like  $\gamma Uv/2$  contain both  $\gamma$  and  $\gamma^2$ , given (2.1). Terms proportional to  $\gamma^2$  are henceforth neglected.

Normal modes are considered, i.e.

$$(u, v, w, p) = (\hat{u}(y), \hat{v}(y), \hat{w}(y), \hat{p}(y))e^{i\alpha x + i\beta z + \sigma t}, \quad (2.5)$$

with  $\alpha$  and  $\beta$  the (real) wavenumbers in the streamwise and spanwise directions, respectively, and  $\sigma$  the (generally complex) amplification factor. This means that the, simpler, case of temporally growing normal modes is adopted, an approach which renders the numerical eigenvalue problem easily tractable.

Introducing (2.5) into (2.4) produces the following set of equations

$$\left\{ \begin{aligned} i\alpha \hat{u} + D\hat{v} + i\beta \hat{w} + \frac{\gamma}{2}\hat{v} - i\alpha \frac{\gamma}{2}y \hat{u} &= 0, \\ \sigma \hat{u} + i\alpha \left(1 - \frac{\gamma y}{2}\right) U \hat{u} + U' \hat{v} + \frac{\gamma}{2}U \hat{v} &= -i\alpha \left(1 - \frac{\gamma y}{2}\right) \hat{p} + \frac{1}{Re} (D^2 - k^2) \hat{u} \\ &+ \frac{\gamma}{Re} \left[ \left(\frac{1}{2}D + y\alpha^2\right) \hat{u} + i\alpha \hat{v} \right], \\ \sigma \hat{v} + i\alpha \left(1 - \frac{\gamma y}{2}\right) U \hat{v} - \gamma U \hat{u} &= -D \hat{p} + \frac{1}{Re} (D^2 - k^2) \hat{v} + \frac{\gamma}{Re} \left[ \left(\frac{1}{2}D + y\alpha^2\right) \hat{v} - i\alpha \hat{u} \right], \\ \sigma \hat{w} + i\alpha \left(1 - \frac{\gamma y}{2}\right) U \hat{w} &= -i\beta \hat{p} + \frac{1}{Re} (D^2 - k^2) \hat{w} + \frac{\gamma}{Re} \left(\frac{1}{2}D + y\alpha^2\right) \hat{w}, \end{aligned} \right. \quad (2.6)$$

with  $k^2 = \alpha^2 + \beta^2$  and  $D = d/dy$ .

## (b) Wall model via thin shell theory

A number of options are available for the model of the compliant coating, comprehensively reviewed by Gad-el-Hak (1986, 2000). Yeo (1992) gives a comparative discussion of volume-based versus surface-based models. In short, volume-based models provide a more realistic treatment of the problem and allow three degrees of freedom in the displacement of each point in the wall. However, they are more difficult to implement numerically. Surface-based models are simpler to use and can still reproduce the salient dynamical features of compliant coatings, since they retain the main ingredients of volume-based approaches: inertia, elasticity and damping. As already stated in the Introduction, the simplicity of surface-based models, which generally allow a single degree of freedom in the wall displacement, has been the main reason for their wide dissemination and use. In the present paper, we have decided to model the compliant walls as spring-backed cylindrical shells, following the lead of Carpenter & Garrad (1985) for an isotropic thin compliant plate. The shells are constrained to move only in the  $y$  direction. We use asterisks to denote dimensional quantities and call  $\eta^*$  the vertical displacement of each wall from its equilibrium position. The equation of motion of the surface can be obtained from Love's thin cylindrical shell theory (Timoshenko & Woinowsky-Krieger 1959)

$$\left[ \left( m^* \frac{\partial^2}{\partial t^{*2}} + d^* \frac{\partial}{\partial t^*} + B^* \Delta_h^2 - T^* \Delta_h + K^* \right) \Delta_h^2 + \frac{E^* H}{R^2} \frac{\partial^4}{\partial z^{*4}} \right] \eta^* = \begin{cases} \Delta_h^2 p^*(h) \\ -\Delta_h^2 p^*(-h) \end{cases}, \quad (2.7)$$

where  $\Delta_h = (\partial^2/\partial x^{*2}) + (\partial^2/\partial z^{*2})$ . In the equation above,  $m^*$  is the plate mass per unit area,  $d^*$  is the wall damping coefficient,  $B^* = (E^* H^3/12(1-\nu^{*2}))$  is the flexural rigidity of the shell, with  $E^*$  the Young modulus,  $H$  the thickness of the shell and  $\nu^*$  Poisson's ratio;  $K^*$  is the spring stiffness and  $T^*$  is the longitudinal tension per unit width. The term on the right-hand side represents the normal stress exerted by the fluid on the shell. For sufficiently large values of the Reynolds number, it has been shown by Nagata & Cole (1999) that the contribution of the normal viscous stresses is negligible: they have thus been omitted from the equations above.

In scaling the wall properties, it is important to adopt reference quantities such that, as the Reynolds number  $Re = U_0 h/\nu$  is varied, the wall maintains the same physical properties. For this, we impose that variations in  $Re$  are only related to changes in the centreline velocity and scale the wall properties with  $h$ ,  $\rho$  and  $\nu$  as

$$m = \frac{m^*}{\rho h}, \quad d = \frac{d^* h}{\rho \nu}, \quad B = \frac{B^*}{\rho \nu^2 h}, \quad E = \frac{E^* h^2}{\rho \nu^2}, \quad K = \frac{K^* h^3}{\rho \nu^2}, \quad T = \frac{T^* h}{\rho \nu^2}.$$

After writing the wall displacement, scaled by  $h$ , as a normal mode in the form  $\eta = \hat{\eta} e^{i\alpha x + i\beta z + \sigma t}$ , the following dimensionless shell equation is found

$$\left[ m\sigma^2 + \frac{d}{Re}\sigma + \frac{1}{Re^2} \left( Bk^4 + Tk^2 + K + \frac{H}{h} \frac{\gamma^2}{4} E \frac{\beta^4}{k^4} \right) \right] \hat{\eta} = \begin{cases} \hat{p}(1) \\ -\hat{p}(-1) \end{cases}. \quad (2.8)$$

This equation differs only in the term proportional to  $\gamma^2$  from that of the thin plate; terms of this same order have been neglected in system (2.6), and the same has thus been done here. This term, which is proportional to  $\gamma^2$ , can be shown to be equal to

$$3(1-\nu^{*2})(h/H)^2(\beta/k)^4 B\gamma^2,$$

and it could become of the same order as  $Bk^4$  when  $k$  becomes  $O(\gamma\beta^2)^{1/4}$ . While this provides no restrictions for the case of spanwise-homogeneous waves, disturbances with  $\alpha=0$  can be considered with the approximation above only if  $\beta$  is larger than  $\gamma^{1/2}$ . All cases reported below have been computed by fixing  $\gamma$  to 0.025, the value used in the experiments by [Matsson & Alfredsson \(1990\)](#) and in the simulations by [Finlay \*et al.\* \(1988\)](#). If  $H/h$  is  $O(1)$ , neglecting the term proportional to  $\gamma^2$  in equation (2.8) is acceptable when  $\alpha=0$  only for spanwise wavenumbers larger than approximately  $10^{-1}$ . The small  $\beta$  limit could be treated by an asymptotic expansion of the governing equations, along the lines of [Phillips & Wu \(1994\)](#); such an expansion has, however, not been attempted since such long-wave modes are of limited interest and can be easily stabilized by small amounts of viscoelastic losses within the walls (cf. [figure 7](#)).

### (c) Boundary conditions

The no-slip condition on the upper wall at  $y=1+\eta$  reads

$$U + u = 0, \quad v = \partial\eta/\partial t, \quad w = 0. \quad (2.9)$$

Linearizing around  $y=1$  we find

$$\hat{u} + \hat{\eta}U' = 0, \quad (2.10)$$

$$\hat{v} - \sigma\hat{\eta} = 0, \quad (2.11)$$

$$\hat{w} = 0, \quad (2.12)$$

and combining (2.10) and (2.11) allows us to eliminate  $\hat{\eta}$

$$\sigma\hat{u} + U'\hat{v} = 0. \quad (2.13)$$

Likewise, introducing (2.10) and (2.11) into (2.8) yields

$$m\sigma\hat{v} + \frac{1}{Re}d\hat{v} - \frac{1}{U'Re^2}(Bk^4 + K + Tk^2)\hat{u} = \hat{p}. \quad (2.14)$$

Hence, the three boundary conditions on  $y=1$  are (2.12)–(2.14). For  $y=-1$ , the same set of equations applies except for the minus sign in front of the pressure term in (2.14). The system of equations (2.6) plus boundary conditions can be reduced to a two-equation set and associated boundary conditions, for example, by eliminating pressure and one velocity component. However, the reduction procedure yields very long-coupled expressions for the two remaining velocity components. To keep things simple, we have preferred to discretize directly the full system, by using a Chebyshev collocation method. Although this doubles the computer memory requirements, we are still largely within the memory limits set by current PCs, even for the better resolved cases. The spectrum of eigenvalues has been explored by employing both global (QZ) and local (Arnoldi) techniques.

The code has been validated by checking results against those for the plane channel flow with compliant walls (Davies & Carpenter 1997a; Nagata & Cole 1999) and curved channel flow with rigid walls (Finlay *et al.* 1988; Matsson & Alfredsson 1990). Furthermore, we have always verified that the  $\sigma$ s of interest were converged to several significant digits.

(d) *The modified Reynolds–Orr energy equation*

Scalar multiplication of the linearized disturbance momentum equation (last three equations of (2.4)) by  $(u, v, w)$  yields the following equation for the disturbance kinetic energy

$$\begin{aligned} \left[ \frac{\partial}{\partial t} + \left(1 - \frac{\gamma}{2}y\right)U \frac{\partial}{\partial x} \right] \left( \frac{1}{2}u_i u_i \right) &= -U'uv - \left(1 - \frac{\gamma}{2}y\right) \frac{\partial(up)}{\partial x} - \frac{\partial(vp)}{\partial y} - \frac{\partial(wp)}{\partial z} \\ &+ \frac{\gamma}{2}(Uuv - pv) + \frac{1}{Re} \frac{\partial}{\partial x_j} \left( u_i \frac{\partial u_i}{\partial x_j} \right) - \frac{1}{Re} \frac{\partial u_i}{\partial x_j} \frac{\partial u_i}{\partial x_j} \\ &+ \frac{\gamma}{Re} \left[ \frac{1}{4} \frac{\partial}{\partial y} (u_i u_i) - y \frac{\partial}{\partial x} \left( u_i \frac{\partial u_i}{\partial x} \right) + y \frac{\partial u_i}{\partial x} \frac{\partial u_i}{\partial x} \right. \\ &\left. + u \frac{\partial v}{\partial x} - v \frac{\partial u}{\partial x} \right], \end{aligned} \tag{2.15}$$

where the repeated suffix convention has been employed. By averaging over a period along  $x$  and  $z$  (the averaging procedure is denoted by overbars) and integrating across the channel, we obtain

$$\begin{aligned} \frac{d}{dt} \int_{-1}^1 \frac{1}{2} \overline{u_i u_i} dy &= \overbrace{- \int_{-1}^1 U' \overline{uv} dy}^{(I1)} - \overbrace{\frac{1}{Re} \int_{-1}^1 \frac{\partial u_i}{\partial x_j} \frac{\partial u_i}{\partial x_j} dy}^{(I2)} \\ &+ \underbrace{\frac{\gamma}{2} \int_{-1}^1 U \overline{uv} dy}_{(G1)} - \underbrace{\frac{\gamma}{2} \int_{-1}^1 \overline{pv} dy}_{(G2)} + \underbrace{\frac{\gamma}{Re} \int_{-1}^1 \left( y \frac{\partial u_i}{\partial x} \frac{\partial u_i}{\partial x} + u \frac{\partial v}{\partial x} - v \frac{\partial u}{\partial x} \right) dy}_{(G3)} \\ &\underbrace{- \overline{vp} \Big|_{-1}^1}_{(C1)} + \underbrace{\frac{1}{Re} \left( u \frac{\partial u}{\partial y} + v \frac{\partial v}{\partial y} \right) \Big|_{-1}^1}_{(C2)} + \underbrace{\frac{\gamma}{4Re} (\overline{u^2} + \overline{v^2}) \Big|_{-1}^1}_{(C3)}. \end{aligned} \tag{2.16}$$

A similar equation, for the case of spatially developing Tollmien–Schlichting waves in a plane channel with finite compliant panels, was derived by Davies & Carpenter (1997b). For the case of the temporal development of disturbance in a boundary layer over a compliant wall, the energy equation was given by Domaradzki & Metcalfe (1987). Compared to these two studies, there are here additional terms arising from the curvature of the channel so that perturbations are not exactly symmetrical (or antisymmetrical) about the channel centreline. The terms labelled with (I1) and (I2) are the classical Reynolds stress production and dissipation terms, respectively. They are typically important in the disturbance energy balance. Other significant terms are those labelled as (C1), (C2) and (G1),

whereas all of the remaining terms are invariably negligible.  $(C1)$  represents the rate of irreversible work done on the wall by the disturbance pressure; it provides a very small contribution to the Dean vortex mode, while it is large for the FISI modes.  $(C2)$  was identified by Carpenter (1990) as an extra-energy removal term for the case of the Tollmien–Schlichting instability. In the present case,  $(C2)$  is positive for the spanwise-periodic surface modes, thus providing energy to the disturbance for all values of the spanwise wavenumber  $\beta$ . In addition,  $(C2)$  feeds energy to the Dean mode at low  $\beta$ s, and drains energy from it after  $\beta$  has exceeded a threshold value. Finally, the term  $(G1)$  is the centrifugal energy production term, always positive—and small—in our case. Although it might be interesting to raise  $\gamma$  and increase the importance of such a term, it should be kept in mind that our equations remain tenable only in the small  $\gamma$  limit.

### 3. Results

The number of parameters at play is very large; hence we have restricted attention to the case of two walls with identical physical and mechanical properties. We will pay particular attention to the effects of the rigidity of the walls (through the flexural rigidity  $B$ ) and to the damping coefficient  $d$ . Following Davies & Carpenter (1997a), the spring stiffness  $K$  is usually taken equal to  $B/4$  (unless otherwise indicated), the mass of each wall takes the value  $m=2$  and the longitudinal tension  $T$  is assumed equal to zero. These assumptions limit somehow the generality of our results, although some numerical tests (not reported here) carried out with different parametric conditions are reassuring as to a wide applicability of the conclusions drawn below.

The relative value of  $K$  versus  $B$  is important since  $\alpha_w = (K/B)^{1/4}$  represents the wavenumber at which free waves in the compliant wall can propagate with minimum possible phase speed. Since a match between a wavenumber characteristic of the coating and one which characterizes fluid-based disturbances could be necessary for the wall to have a significant effect on the fluid,  $\alpha_w$  will also be allowed to vary, to assess whether some wall parameters can be found that maximally affect Dean vortices.

#### (a) Streamwise-homogeneous disturbances

We are first concerned with the effect of compliant coatings on modes with  $\alpha=0$ . The Dean vortex mode belongs to this class. Representative neutral curves for different values of  $K$  and in the absence of viscous damping are shown in figure 2a. For  $K$  larger than  $10^5$ , the curves are indistinguishable from that of the rigid-wall case. As the walls become softer, two phenomena occur: (i) Dean modes are destabilized at smaller values of the Reynolds number, for  $\beta$ s below the critical value of the rigid-wall case and (ii) for even larger spanwise wavelengths, the Dean instability is preceded by a weakly amplified surface wave (simply labelled as FISI, grey regions in the figure 2). Hence, as far as a delay of the Dean instability is concerned, the adoption of flexible walls with the characteristics indicated has, at best, no effect for  $\beta$  larger than two. Conversely, if the walls are too soft, for example, when coatings made from household gelatin or a PVC plastisol (Gad-el-Hak 1986) are employed, a long spanwise wave surface-based mode can be excited at very low  $Re$ . Numerical results obtained for

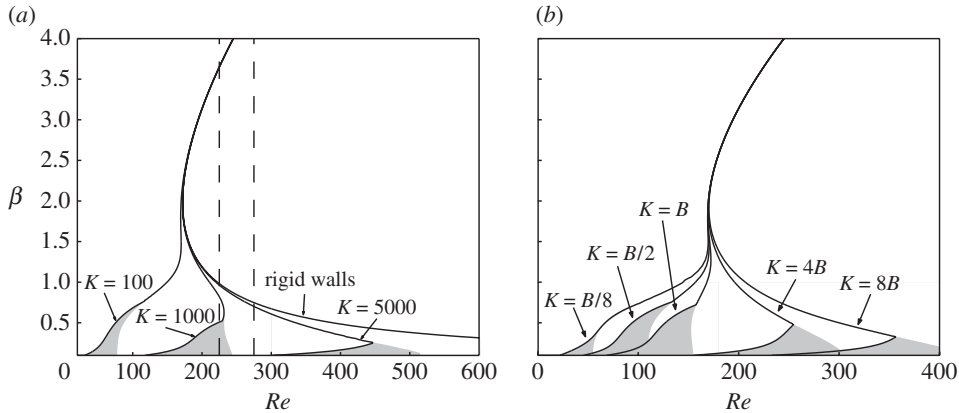


Figure 2. Neutral curves showing the effect of wall compliance on streamwise homogeneous disturbances. The grey regions correspond to an unstable spanwise-periodic FISIs. The damping coefficient  $d$  is taken equal to zero. (a)  $K=B/4$ ; vertical dashed lines are drawn for  $Re=225$  and  $Re=275$ . (b)  $B=400$ , effect of varying  $K$ .

decreasing values of  $\beta$  suggest that the critical spanwise wavenumber of the travelling wave tends to zero, which would correspond to a mode with no horizontal structure. However, modes with  $\beta \rightarrow 0$  are outside of the domain of validity of our equations (see discussion at the end of §2*b*). Furthermore, the numerical search of solutions characterized by  $\alpha=0$  and very small  $\beta$ s is very difficult owing to the stiffness of the equations, with the spanwise velocity  $\hat{w}$  that progressively decouples from the other dependent variables as the spanwise wavenumber decreases. On the other hand, as already anticipated, such low- $\beta$  modes are immediately stabilized by the presence of even a weak damping in the wall. Further tests demonstrate that the onset of FISIs modes is delayed when the curvature parameter is decreased.

The influence of  $\alpha_w$  is investigated in figure 2*b* via variations of the spring stiffness  $K$  for a flexural rigidity fixed at  $B=400$ . An increase in spring stiffness has a stabilizing effect on both large-wavelength Dean vortices and FISIs. Additionally, the broadest region of destabilized wavenumbers for the spanwise-periodic surface modes corresponds to the case  $K \approx B$  (i.e.  $\alpha_w \approx 1$ ); this unstable region shrinks with either an increase or a decrease of  $K$  and remains localized in a region of small  $\beta$ , reflecting a weak coupling between the characteristic coating length ( $\alpha_w^{-1}$ ) and the wavelength of the Dean modes.

In figure 3*a*, we have fixed  $Re=225$ ,  $K=1000$  and  $B=4000$  and spanned the  $\beta$  range from 0.1 to 2.0, plotting all the points of the spectrum. Three modes are clearly identified, labelled in figure 3*a* as ‘Dean vortex’, ‘FISI1’ and ‘FISI2’. The latter mode is damped for all  $\beta$ s; the other two exhibit opposite behaviours with the increase of the spanwise wavenumber. For  $\beta$  larger than approximately 0.75, the growth rate of the steady Dean mode exceeds that of the FISI1 mode. This is confirmed by the plot of the amplification rate ( $2\sigma$ ) of the disturbance kinetic energy  $E_k$  versus  $\beta$  displayed in figure 3*b*. The Dean mode becomes unstable for  $\beta$  larger than 0.82 and achieves its maximum amplification at  $\beta=2.22$ . Although for small  $\beta$ s, the FISI1 mode is dominant, its amplification factor remains very small and the mode is unlikely to be responsible for transition in practical applications.

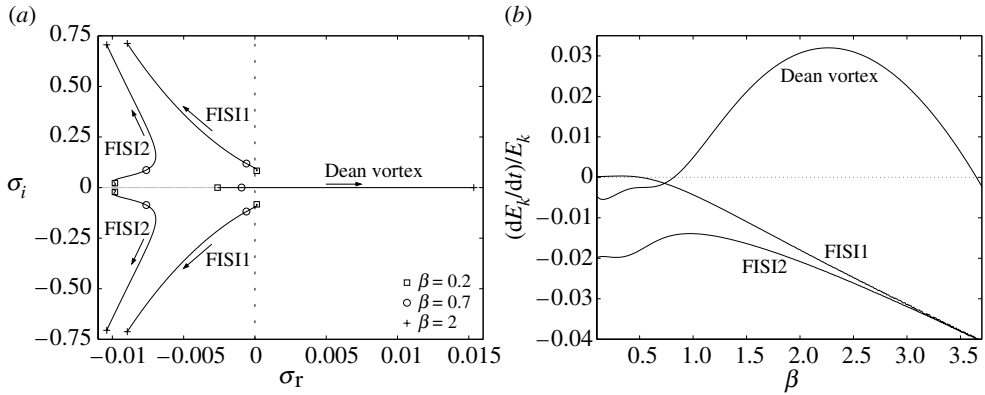


Figure 3. (a) Eigenvalue spectrum showing the evolution of the main streamwise homogeneous eigenmodes with the spanwise wavenumber ( $0.1 \leq \beta \leq 2$ ) and (b) disturbance kinetic energy growth rate versus spanwise wavenumber ( $0.1 \leq \beta \leq 3.7$ ) for the same modes. Arrows denote increasing  $\beta$ . The parameters are  $Re=225$ ,  $K=1000$ ,  $B=4000$  and  $d=0$ .

Interestingly, two such surface modes appear simultaneously with opposite phase velocities and their superposition could yield a standing wave. To assess the direction in which the energy of the FIS11 modes propagates, the group velocity must be computed. For example, for the parameters of figure 3a, when  $\alpha=0$  and  $\beta=0.2$ , the phase speed along  $z$  is  $c_z = \pm 0.414$ , whereas the two components of the group velocity are  $c_{gx} = -\partial\sigma_i/\partial\alpha = 0.2407$  and  $c_{gz} = -\partial\sigma_i/\partial\beta = \pm 0.0136$ . Thus, in general, long-wave spanwise-periodic surface-based instabilities transport energy obliquely in the  $(x, z)$  plane.

In figure 4, the terms contributing the most to the energy budget of the spanwise-periodic FIS11 mode are plotted as function of  $\beta$ . The figure demonstrates that the budget is dominated by the terms denoted by (I2), (C1) and (C2), with the latter two terms always destabilizing. Analysis of the individual contributions reveals that all the terms which depend on  $\gamma$  have no influence in the balance, and that (C2) is the main source of energy up to  $\beta$  equal to approximately 2.2. As the waves become shorter (in  $z$ ), the work done on the wall by the disturbance pressure, term (C1), contributes the most to the disturbance energy balance, with a strong damping effect provided by viscous dissipation, through term (I2).

At slightly larger values of  $Re$ , the FIS11 mode is damped and the Dean vortex dominates. The total kinetic energy and the main terms of the energy balance for the Dean mode are calculated for  $Re=275$  and compared to the rigid-wall case in figure 5. The most important terms are (I1), (I2) and (C2), with (C2) stabilizing (like for Tollmien–Schlichting waves, Carpenter 1990) except for the case of vortices elongated in  $z$ . The comparison with the rigid-wall case indicates that the destabilization of the large-wavelength modes is not due to an increase of energy production by the Reynolds stresses (I1), contrary to what happens for Tollmien–Schlichting waves or crossflow vortices (Cooper & Carpenter 1997a). The major influence of wall compliance occurs through a decrease of viscous dissipation (I2) and the appearance of (C2), destabilizing for small values of  $\beta$ .

The shapes of the different modes are displayed in figure 6, for the same parameter values as in figure 3a for  $\beta=0.7$ . The streamwise  $\hat{u}$  and wall-normal  $\hat{v}$

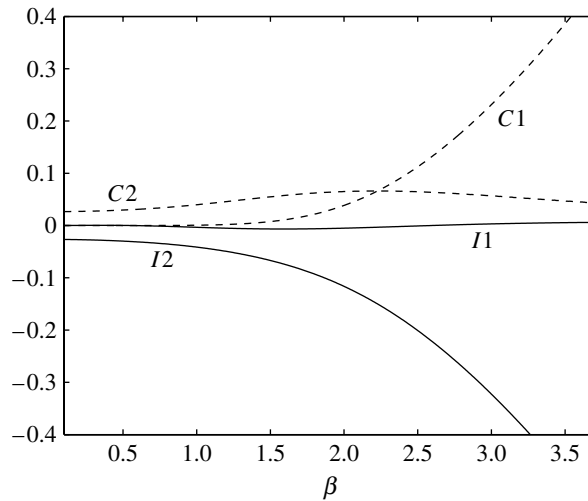


Figure 4. Main terms in the disturbance energy balance, normalized by  $E_k$  for the FIS11 mode; same parameters as in figure 3*b*.

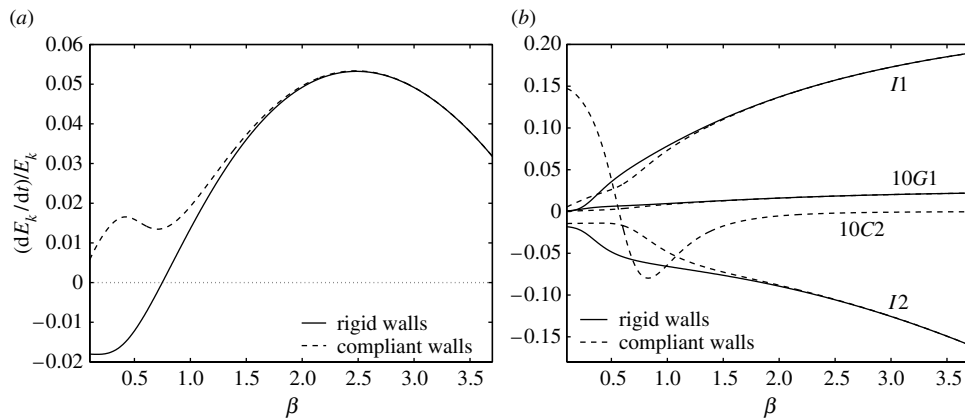


Figure 5. (a) Disturbance energy growth rate versus spanwise wavenumber and (b) main terms in the disturbance energy balance for the Dean vortex mode. All terms are normalized by  $E_k$ . The parameters are  $Re=275$ ,  $K=1000$ ,  $B=4000$  and  $d=0$ .

velocity shapes for the Dean vortices resemble those for the rigid-wall case, aside from the behaviour in the vicinity of the walls. FISIs exhibit, as it could have been expected, velocity peaks in correspondence of  $y = \pm 1$ .

Kramer's surfaces typically include a viscous fluid substrate through the presence of the coefficient  $d$  in equation (2.8) (Carpenter & Garrad 1985). The effect of this parameter can be assessed from figure 7. The surface-based mode present when  $d=0$  disappears in the presence of damping; the neutral curves for various values of  $d \neq 0$  are all superposed to one another and correspond to stationary streamwise vortices. The effect of  $d$  appears when attention shifts from marginal curves to isolines of constant  $\sigma_r \neq 0$ . For example, when  $\sigma_r=0.01$ , the figure shows that modes with low  $\beta$ s are stabilized by damping. For  $d=1000$ , the curve of constant amplification approaches that for the rigid-wall case.

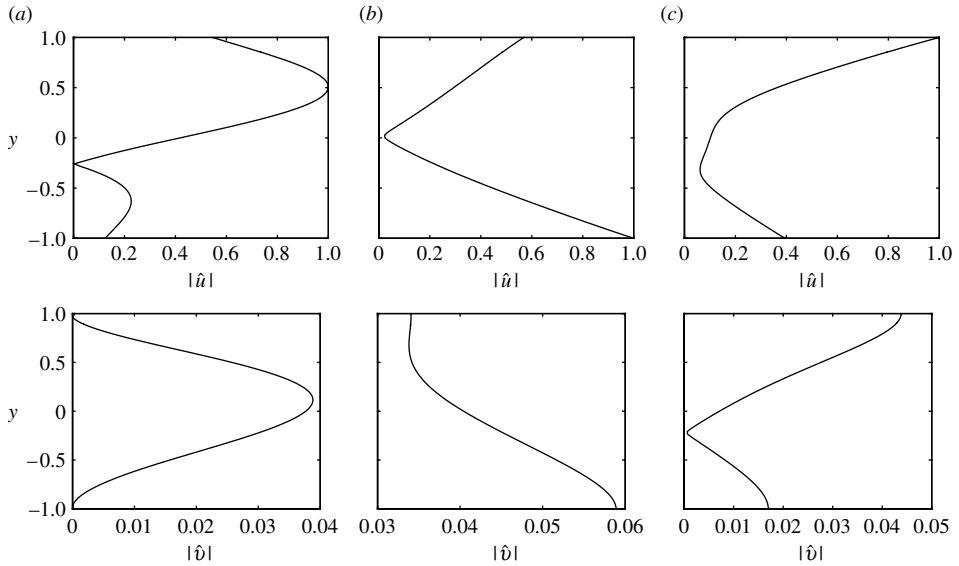


Figure 6. Longitudinal  $\hat{u}$  and wall normal  $\hat{v}$  velocities (absolute values normalized by  $\hat{u}$  maximum) for the case shown in figure 3a with  $\beta=0.7$ . (a) Stable Dean vortex, (b) stable FIS1 and (c) stable FIS2.

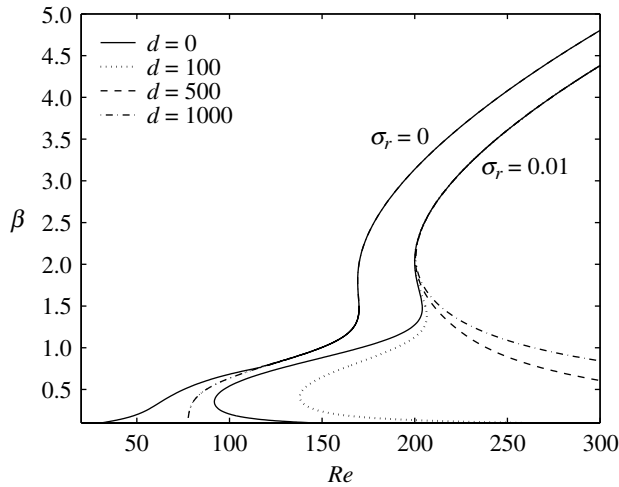


Figure 7. Neutral curves and curves of constant growth rate ( $\sigma_r=0.01$ ) for different damping coefficients. The parameters are  $K=100$  and  $B=400$ .

The results obtained demonstrate that compliance does not stabilize longitudinal vortex structures induced by centrifugal forces; this is in contradiction with the limited experimental data available (Yurchenko & Babenko 1987). The experiments by Yurchenko & Babenko (1987) dealt with near-wall Görtler vortices and the presence of slip boundaries has an influence in their case. The effect of compliance on near-wall flow structures is confirmed by the measurements by Choi *et al.* (1997), where a 7% drag reduction is found for the case of a turbulent boundary layer. The different behaviour encountered here is noteworthy; it must probably be ascribed to the fact that Dean vortices are not confined to a thin, near-wall layer.

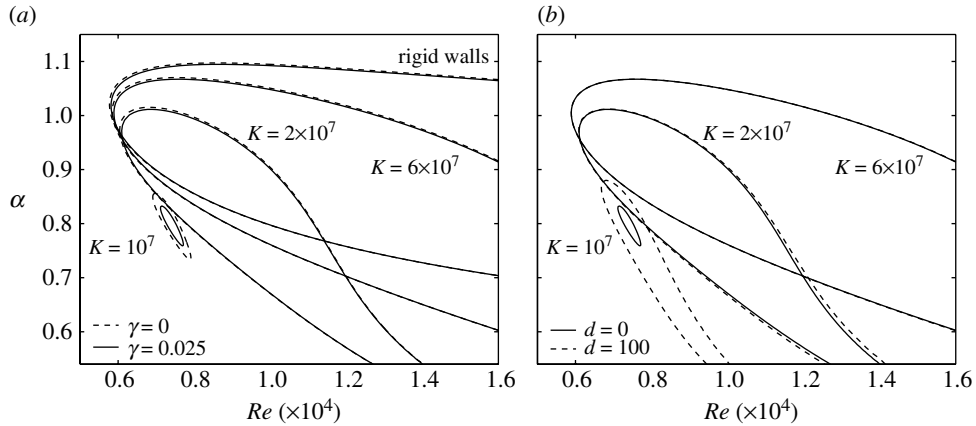


Figure 8. Neutral curves for the Tollmien–Schlichting instability showing the effect of (a) wall compliance and wall curvature for  $d=0$  and (b) wall damping for  $\gamma=0.025$ . In both cases, we have  $B=4K$ .

Since transition in wall-bounded shear flows is linked to the receptivity conditions, and waves with  $\alpha$  different from zero might be excited by the environment, it is worthwhile to extend the investigation to different kinds of modes.

### (b) *Spanwise-homogeneous disturbances*

The results for waves with  $\beta=0$  are very similar to those of the plane channel case. The effect of curvature on the marginal stability of Tollmien–Schlichting modes can be inferred from examination of figure 8a. When  $d=\gamma=0$ , the results in the figure are identical to those reported by Davies & Carpenter (1997a) (cf. their figure 1). Notably, increased wall compliance shrinks the marginal curve, forcing it to close into a single loop. This stabilizing effect is further enhanced by curvature, whereas damping (cf. Figure 8b) is destabilizing, and more so for increasing compliance.

Besides the viscous mode, wall-based instabilities may appear, such as TWF (Carpenter & Garrad 1985, 1986). Like for the case  $\alpha=0$ , wall damping tends to reduce the amplification of surface-based modes. In the present case, the TWF has been classified into two categories, quasi-symmetrical (STWF) and quasi-antisymmetrical (ATWF), with the prefix ‘quasi’ stemming from the presence of curvature. The study of Davies & Carpenter (1997a) for the case of the plane channel focused on TWF with the same parity as the Tollmien–Schlichting instability, e.g.  $\hat{v}$  is symmetric about the channel centreline.

However, it has been clear since Nagata & Cole (1999) that antisymmetric TWF modes always become unstable before their symmetric counterparts, at least for the same parameters considered by Davies & Carpenter (1997a) (it should also be observed that the labels in fig. 1 of the paper by Nagata & Cole are misplaced; they should be, from top to bottom, (b), (c) and (a)). The situation is similar when the channel is curved, and the neutral curves are but slightly displaced with respect to the plane case. The spectrum in figure 9 pertains to the case  $\alpha=1$  and it reveals that two TWF modes of positive phase velocity, i.e.

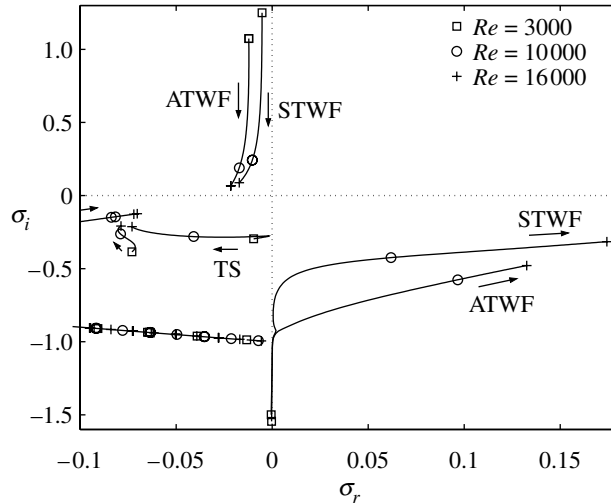


Figure 9. Eigenvalue spectrum showing the evolution of the main spanwise homogeneous eigenmodes with Reynolds number ( $3000 \leq Re \leq 16\,000$ ) for a fixed streamwise wavenumber  $\alpha = 1$ . The modes of interest are labelled ATWF (quasi-antisymmetric travelling-wave flutter), STWF (quasi-symmetric travelling-wave flutter) and TS (Tollmien-Schlichting mode). Arrows denote increasing  $Re$ . The untensioned wall is defined by the parameters:  $K = 10^7$ ,  $B = 4K$ ,  $m = 2$ .

negative  $\sigma_i$ , remain very close to the imaginary  $\sigma$  axis (rendering difficult the numerical identification of the neutral curve) in a large range of Reynolds numbers ( $3000 < Re < 5000$ ), before the growth rate of the ATWF mode starts increasing in a clear manner. At  $Re = 10\,000$ , it is the quasi-antisymmetric wave that exhibits the largest amplification; when  $Re$  has increased to the value of  $16\,000$  the quasi-symmetric mode grows faster. For the untensioned wall considered, the phase velocity of the STWF modes at each value of  $Re$  is well approximated by the relation proposed by Davies & Carpenter (1997a) for the critical speed of travelling flutter modes, i.e.

$$c_m = \frac{1}{Re} \left[ \frac{4KB}{(m + 1/5)^2} \right]^{1/4}.$$

In the  $Re$  range considered, the TS-mode is always stable. Furthermore, two upstream TWF modes are present in the spectrum; they are damped, and increasingly so with the increase of  $Re$ . The eigenfunctions of the two unstable TWF modes at  $Re = 10\,000$  are plotted in figure 10. These plots show that in both cases the flow is separated into two regions: an almost parallel core region and a near-wall flow region. Quasi-symmetric and antisymmetric pressure fluctuations produce oscillations of the walls, which propagate downstream at speeds close to the bulk speed.

Isolines of amplification rate in the  $\alpha$ - $Re$  plane are provided in figure 11. The left frame, obtained for  $K = 10^7$ , makes clear that transition can be initiated by the quasi-antisymmetric instability waves. The kinks in the isolines reveal the points where the growth of the quasi-symmetric TWF mode overtakes that of the ATWF. On the right frame, for the case of larger spring stiffness, we observe that

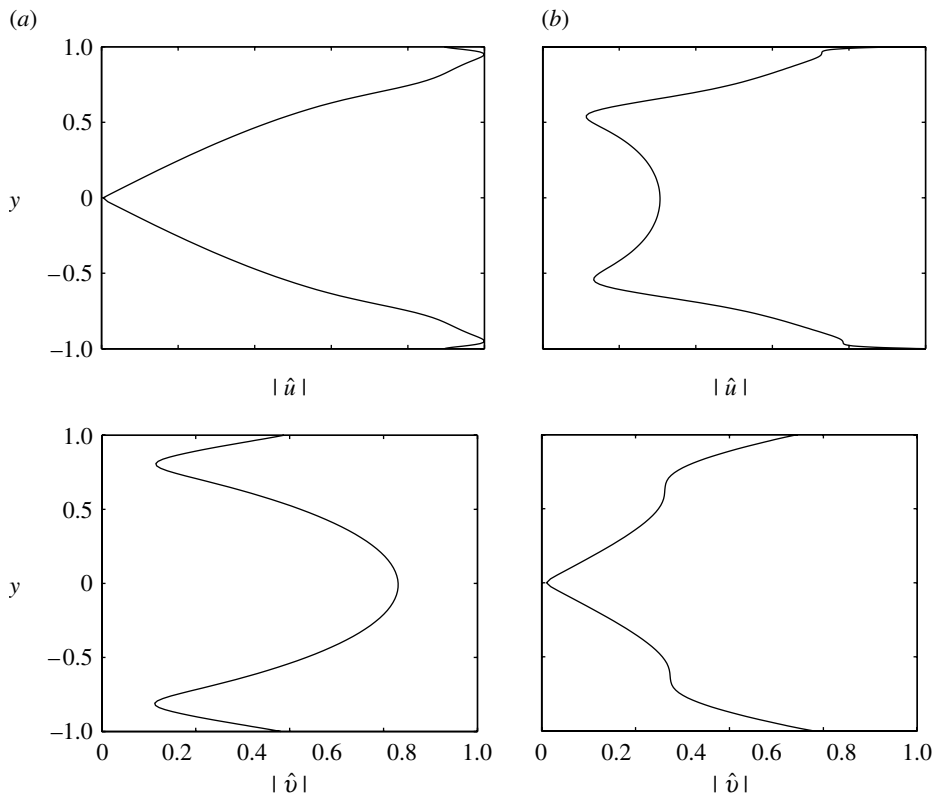


Figure 10. Plots of the unstable (a) STWF and (b) ATWF modes at  $Re=10\,000$ . Other parameters are as in figure 9.

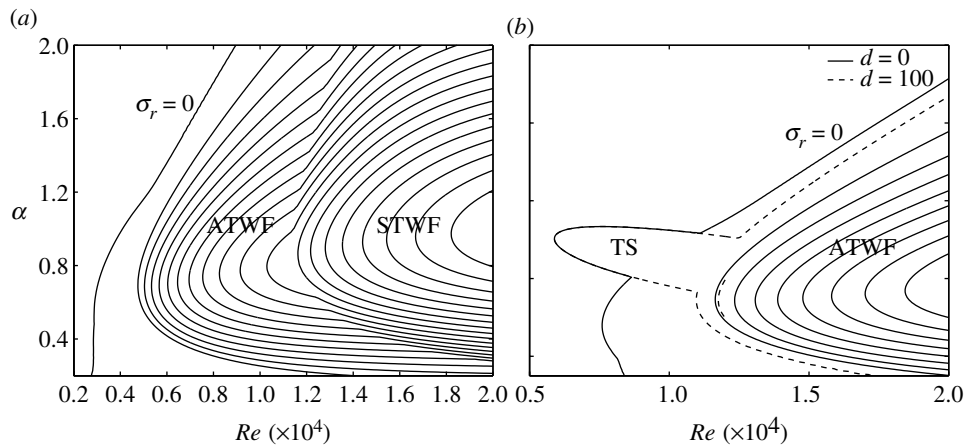


Figure 11. Curves of constant positive growth rate (lines are equally spaced by  $\Delta\sigma_r=0.01$ ) for spanwise homogeneous disturbances showing the dominant modes with (a)  $K=10^7$ ,  $B=4 \times 10^7$  and (b)  $K=6 \times 10^7$ ,  $B=24 \times 10^7$ . In (b), the effect of wall damping is also shown.

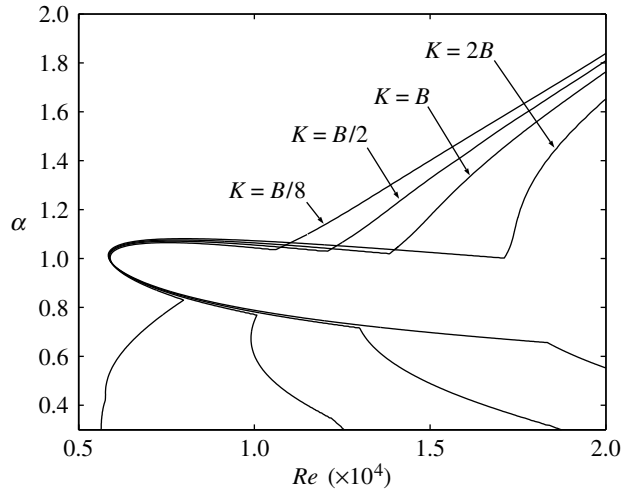


Figure 12. Neutral curves showing the influence of the spring stiffness on spanwise homogeneous disturbances for a fixed flexural rigidity  $B=24 \times 10^7$  with  $d=0$ .

the TS mode occurs earlier than the streamwise-travelling wall-based modes. For larger values of  $Re$ , the quasi-antisymmetric mode (which is but mildly delayed by damping, whereas the TS mode is practically unaffected) is capable of destabilizing waves in a large range of wavenumbers. Quasi-symmetric modes become dominant for  $Re$  exceeding 20 000 (not shown in the figure).

The influence of  $\alpha_w$  is considered in figure 12 for a flexural rigidity fixed at  $B=24 \times 10^7$ . Like for the case of the spanwise-periodic surface waves, the TWF modes are stabilized by an increase in spring stiffness. Conversely, TS waves are only slightly destabilized.

To conclude this section, we observe that TWF modes can completely overrule Tollmien–Schlichting instabilities and be the primary causes of transition when the compliance of the wall is increased. However, by comparison with the results of the previous section, it is evident that very soft coatings would be required for TWF to become ‘competitive’ with the Dean vortex mode in triggering transition for the value of  $\gamma$  considered. As far as transition delay is concerned, also for the case of spanwise-homogeneous disturbances, there is not much of a case for wall coating, at least in the isotropic form proposed here, owing to the premature appearance of surface-based instabilities.

### (c) Three-dimensional disturbances

With the scalings employed for the coating properties, a generalization of Squire’s theorem applies to the plane channel case so that attention can be focused on the case of two-dimensional disturbances (Rotenberry & Saffman, 1990; Davies & Carpenter 1997a). When curvature is present, no such theorem applies and the behaviour of three-dimensional waves must be studied. The results shown in figure 13 pertain to the rigid-wall cases and provide a reference against which subsequent results can be compared. The figure shows that when oblique modes are excited by the receptivity conditions, steady vortices are

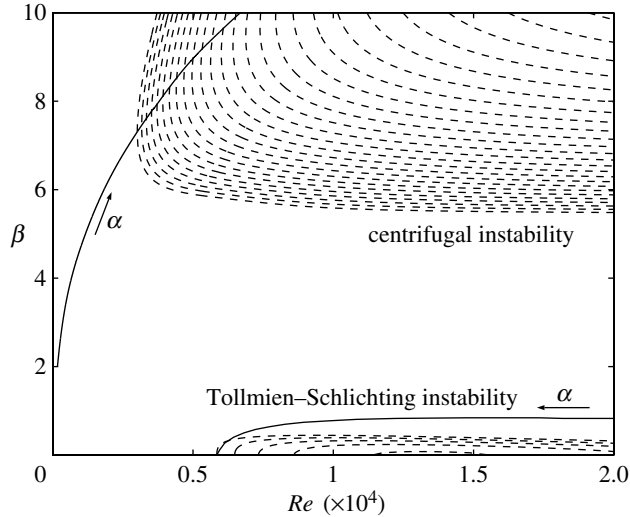


Figure 13. Three-dimensional modes in the  $Re$ - $\beta$  plane for the curved channel with rigid walls, featuring centrifugal and Tollmien-Schlichting instabilities. Solid line represents evolution of the critical point for both instabilities with wave number  $\alpha$  (centrifugal instability,  $0 \leq \alpha \leq 1.6$ ; Tollmien-Schlichting instability,  $0.37 \leq \alpha \leq 1.018$ ). Arrows point in the directions of increasing  $\alpha$  for each mode. Dashed lines represent the curves of constant positive growth rate (spacing between adjacent lines is 0.001) for the case  $\alpha=1$ .

progressively stabilized when  $\alpha$  increases. This indicates that a Squire-like theorem applies, i.e. that in centrifugally unstable flows the critical conditions can be obtained from consideration of two-dimensional modes with  $\alpha=0$ . Conversely, as  $\alpha$  is raised above zero, the viscous TS mode is destabilized initially, with a subsequent stabilization for larger  $\alpha$  values. Critical conditions are found for  $Re_c=5814$  and  $\alpha_c=1.018$  when  $\beta$  vanishes. Comparing the growth rates of the two modes for all possible orientations of the horizontal wavevector shows that the centrifugal mode is never overruled by the viscous mode. For this to occur,  $\gamma$  should be taken smaller than  $2 \times 10^{-5}$ .

Also in the presence of wall compliance, the viscous instability becomes irrelevant in bringing about transition, owing to the appearance of surface-based modes. For small values of  $\alpha$ , the situation is qualitatively similar to that treated in §3*a*; for large values of  $\alpha$  compared with  $\beta$ , the behaviour can be reconducted to that described in §3*b*. The intermediate situation of  $\alpha=1$  is considered in figure 14, where curves of constant amplification factor  $\sigma_r$  are displayed in the  $\beta$ - $Re$  plane for different values of the spring stiffness  $K$ . For the case of very soft coatings ( $K=10^3$ ), a TWF mode disposed obliquely in the horizontal plane emerges as the main cause of instability for  $Re$  as low as 28. The centrifugal mode is dominant only when  $\beta$  is larger than 6; it grows much more slowly than the surface-based mode (as it can be easily inferred by comparing the spacing between isolines for the two cases). Increasing the spring stiffness has a negligible influence on the centrifugal mode, whereas the onset of the rapidly growing flow-induced surface instability is shifted to higher values of the Reynolds number.

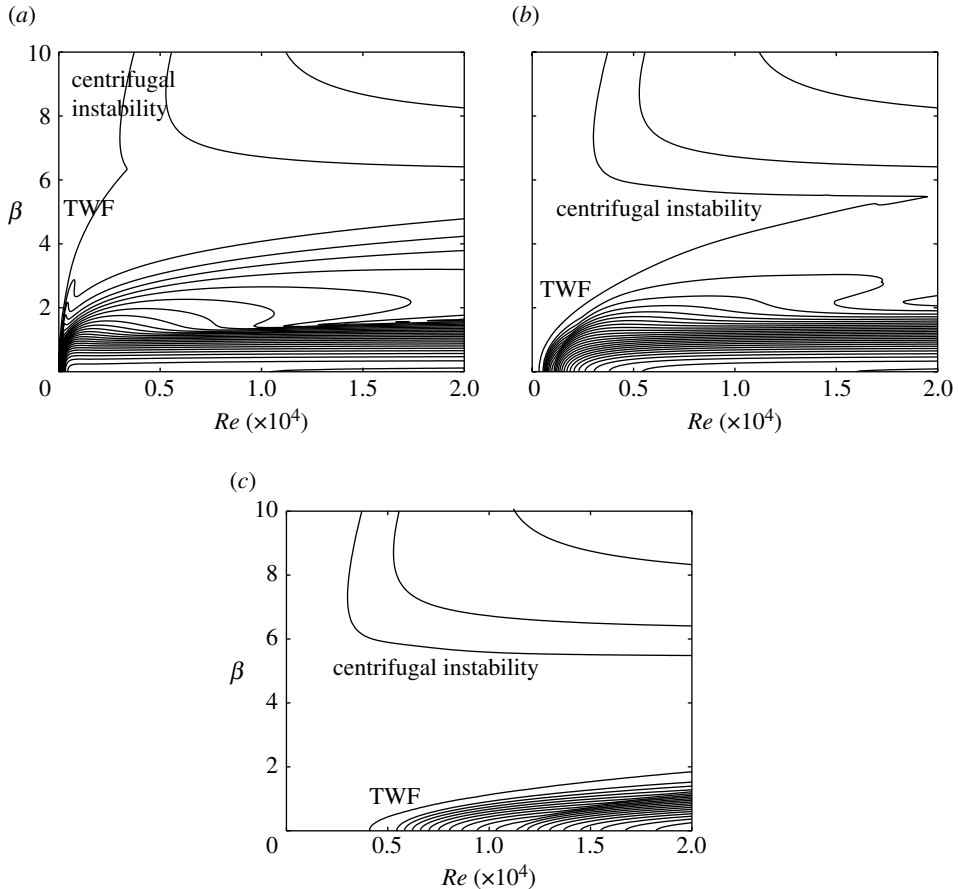


Figure 14. Curves of constant positive growth rate (lines are equally spaced by  $\Delta\sigma_r=0.01$ ) showing the dominant modes for waves with  $\alpha=1$  in a curved compliant channel: (a)  $K=10^3$ , (b)  $K=10^5$  and (c)  $K=10^7$ . In all cases, we have  $B=4K$ .

#### 4. Conclusions

A study of the different modes of instability occurring in a curved channel equipped with Kramer-type walls has been conducted. The compliant surfaces have been treated as thin elastic shells supported by rigid frames through arrays of springs, following a procedure initiated by Benjamin (1960) and Landahl (1962) and perfected by Peter Carpenter and co-workers in a long series of publications.

As far as hydrodynamic modes are concerned, it is found that wall compliance has a noticeable effect on both Dean and TS waves. Long-wavelength Dean modes are destabilized by soft coating by the combined action of the Reynolds stress production term (term (I1) in equation (2.16)) and the term of diffusion of momentum from the wall (term (C2)). For sufficiently large values of the spanwise wavenumber  $\beta$ , no differences are found when compared with the rigid-wall Dean case. The influence of compliance on the Tollmien–Schlichting instability is the same as in the plane channel case and soft coatings can completely stabilize the mode, provided that wall damping remains small.

The importance of compliance is manifest in the appearance of hydroelastic modes, and in this problem a long spanwise-periodic surface instability has been discovered. Such a mode appears in the small  $\beta$  limit owing to the diffusion of momentum from the flexible wall towards the fluid (the disturbance energy source term is  $(C2)$ ). The mode is weakly amplified and it transports energy both along  $x$  and  $z$ ; its growth is reduced by viscoelastic losses in the wall or by lowering the curvature parameter  $\gamma$ . When two-dimensional spanwise homogeneous disturbances are focused upon, the results conform to those of the plane channel case; the importance of considering quasi-antisymmetric  $\hat{v}$ -modes in the analysis of TWF instabilities has been highlighted.

Despite the large number of parameters at play, we have conducted a rather extensive parametric investigation, without ever being able to identify SD modes or the occurrence of absolutely unstable coalescing modes. The present problem appears thus to give rise uniquely to convective instabilities so that the environment crucially determines structure and orientation of the developing perturbations. A receptivity analysis of this flow following the lead of Luchini & Bottaro (1998) could provide useful indications on the initial conditions more likely to provoke transition. Another interesting line of research concerns the study of hydrodynamic and hydroelastic modes in a boundary layer over a curved compliant wall; if such instabilities are of convective nature—as the present study suggests for the related case of the curved channel flow—their study could be conducted on the basis of the parabolic equations derived by Hall (1983).

We thank Mohamed Gad-el-Hak for interesting discussions on the topic of this paper and Francesco Asuni for his help with some numerical calculations. A.G. has been supported during her stay in Genova by a Marie Curie Early Stage Training grant through the FLUBIO project (MEST-CT-2005-020228).

## References

- Allen, L. & Bridges, T. J. 2003 Flow past a swept wing with a compliant surface: stabilizing the attachment-line boundary layer. *Stud. Appl. Math.* **110**, 333–349. (doi:10.1111/1467-9590.00241)
- Benjamin, T. B. 1960 Effects of a flexible boundary on hydrodynamic stability. *J. Fluid Mech.* **9**, 513–532. (doi:10.1017/S0022112060001286)
- Carpenter, P. W. 1990 Status of transition delay using compliant walls. In *Viscous drag reduction in boundary layers* (eds D. M. Bushnell & J. N. Hefner), pp. 79–113. Washington, DC: American Institute of Aeronautics and Astronautics, Inc.
- Carpenter, P. W. & Garrad, A. D. 1985 The hydrodynamic stability of flow over Kramer-type compliant surfaces. Part 1. Tollmien–Schlichting instabilities. *J. Fluid Mech.* **155**, 465–510. (doi:10.1017/S0022112085001902)
- Carpenter, P. W. & Garrad, A. D. 1986 The hydrodynamic stability of flow over Kramer-type compliant surfaces. Part 2. Flow-induced surface instabilities. *J. Fluid Mech.* **170**, 199–232. (doi:10.1017/S002211208600085X)
- Carpenter, P. W., Davies, C. & Lucey, A. D. 2000 Hydrodynamics and compliant walls: does the dolphin have a secret? *Curr. Sci.* **79**, 758–765.
- Choi, K.-S., Yang, X., Clayton, B. R., Glover, E. J., Atlar, M., Semenov, B. N. & Kulik, V. M. 1997 Turbulent drag reduction using compliant surfaces. *Proc. R. Soc. A* **453**, 2229–2240. (doi:10.1098/rspa.1997.0094)
- Cooper, A. J. & Carpenter, P. W. 1997a The stability of rotating-disc boundary-layer flow over a compliant wall. Part 1. Type I and II instabilities. *J. Fluid Mech.* **350**, 231–259. (doi:10.1017/S0022112097006976)

- Cooper, A. J. & Carpenter, P. W. 1997*b* The stability of rotating-disc boundary-layer flow over a compliant wall. Part 2. Absolute instability. *J. Fluid Mech.* **350**, 261–270. (doi:10.1017/S0022112097006964)
- Davies, C. 2003 Convective and absolute instabilities of flow over compliant walls. In *IUTAM Symp. Flow past highly compliant boundaries and in collapsible tubes* (eds P. W. Carpenter & T. J. Pedley), pp. 69–93. Dordrecht, The Netherlands: Kluwer Academic Publisher.
- Davies, C. & Carpenter, P. W. 1997*a* Instabilities in a plane channel flow between compliant walls. *J. Fluid Mech.* **352**, 205–243. (doi:10.1017/S0022112097007313)
- Davies, C. & Carpenter, P. W. 1997*b* Numerical simulation of the evolution of Tollmien–Schlichting waves over finite compliant panels. *J. Fluid Mech.* **335**, 361–392. (doi:10.1017/S0022112096004636)
- Davies, C. & Carpenter, P. W. 2001 A novel velocity-vorticity formulation of the Navier–Stokes equations with applications to boundary layer disturbance evolution. *J. Comput. Phys.* **172**, 119–165. (doi:10.1006/jcph.2001.6817)
- Davies, C. & Carpenter, P. W. 2003 Global behaviour corresponding to the absolute instability of the rotating-disc boundary layer. *J. Fluid Mech.* **486**, 287–329. (doi:10.1017/S0022112003004701)
- Dean, W. R. 1928 Fluid motion in a curved channel. *Proc. R. Soc. A* **121**, 402–420. (doi:10.1098/rspa.1928.0205)
- Denier, J. P. & Hall, P. 1991 The effect of wall compliance on the Görtler vortex instability. *Phys. Fluids A* **3**, 2000–2002. (doi:10.1063/1.857932)
- Domaradzki, J. A. & Metcalfe, R. W. 1987 Stabilization of laminar boundary layers by compliant membranes. *Phys. Fluids* **30**, 695–705. (doi:10.1063/1.866320)
- Finlay, W. H., Keller, J. B. & Ferziger, J. H. 1988 Instability and transition in curved channel flow. *J. Fluid Mech.* **194**, 417–456. (doi:10.1017/S0022112088003052)
- Gad-el-Hak, M. 1986 The response of elastic and viscoelastic surfaces to a turbulent boundary layer. *J. Appl. Mech.* **53**, 206–212.
- Gad-el-Hak, M. 2000 *Flow control. Passive, active, and reactive flow management*. Cambridge, UK: Cambridge University Press.
- Gray, J. 1936 Studies in animal locomotion. VI. The propulsive power of dolphins. *J. Exp. Biol.* **13**, 192–199.
- Hall, P. 1983 The linear development of Görtler vortices in growing boundary layers. *J. Fluid Mech.* **130**, 41–58. (doi:10.1017/S0022112083000968)
- Kramer, M. O. 1957 Boundary-layer stabilization by distributed damping. *J. Aerosp. Sci.* **24**, 459–460.
- Kramer, M. O. 1960 Boundary-layer stabilization by distributed damping. *J. Am. Soc. Navig. Eng.* **72**, 25–33.
- Landahl, M. T. 1962 On the stability of a laminar incompressible boundary layer over a flexible surface. *J. Fluid Mech.* **13**, 609–632. (doi:10.1017/S002211206200097X)
- Luchini, P. & Bottaro, A. 1998 Görtler vortices: a backward-in-time approach to the receptivity problem. *J. Fluid Mech.* **363**, 1–23. (doi:10.1017/S0022112098008970)
- Matsson, O. J. E. & Alfredsson, P. H. 1990 Curvature and rotation induced instabilities in channel flow. *J. Fluid Mech.* **210**, 537–563. (doi:10.1017/S0022112090001392)
- Nagata, M. & Cole, T. R. 1999 On the stability of plane Poiseuille flow between compliant boundaries. In *Proc. Int. Conf. Computational methods and experimental measurements IX, Naples, Italy* (eds G. M. Carlomagno & C. A. Brebbia), pp. 231–240. Southampton, UK: WIT Press.
- Phillips, W. R. C. & Wu, Z. 1994 On the instability of wave-catalysed longitudinal vortices in strong shear. *J. Fluid Mech.* **272**, 235–254. (doi:10.1017/S0022112094004453)
- Rotenberry, J. M. & Saffman, P. G. 1990 Effect of compliant boundaries on weakly nonlinear shear waves in channel flow. *SIAM J. Appl. Math.* **50**, 361–394. (doi:10.1137/0150023)
- Timoshenko, S. & Woinowsky-Krieger, S. 1959 *Theory of plates and shells*. New York, NY: McGraw-Hill.

- Wiplier, O. & Ehrenstein, U. 2001 On the absolute instability in a boundary-layer flow with compliant coatings. *Eur. J. Mech. B: Fluids* **20**, 127–144. (doi:10.1016/S0997-7546(00)01107-9)
- Xu, S., Rempfer, D. & Lumley, J. 2003 Turbulence over a compliant surface: numerical simulation and analysis. *J. Fluid Mech.* **478**, 11–34. (doi:10.1017/S0022112002003324)
- Yeo, K. S. 1988 The stability of boundary-layer over single- and multi-layer viscoelastic walls. *J. Fluid Mech.* **196**, 359–408. (doi:10.1017/S0022112088002745)
- Yeo, K. S. 1990 The hydrodynamic stability of boundary-layer flow over a class of anisotropic compliant walls. *J. Fluid Mech.* **220**, 125–160. (doi:10.1017/S0022112090003214)
- Yeo, K. S. 1992 The three-dimensional stability of boundary-layer flow over compliant walls. *J. Fluid Mech.* **238**, 537–577. (doi:10.1017/S0022112092001812)
- Yeo, K. S. 1994 Note on the inviscid stability of flow over compliant wall. *J. Fluid Mech.* **279**, 165–168. (doi:10.1017/S002211209400385X)
- Yeo, K. S. & Dowling, P. 1987 The stability of inviscid flows over passive compliant walls. *J. Fluid Mech.* **183**, 265–292. (doi:10.1017/S0022112087002635)
- Yeo, K. S., Khoo, B. C. & Chong, K. 1994 The linear stability of boundary-layer over compliant walls: effects of boundary-layer growth. *J. Fluid Mech.* **280**, 199–225. (doi:10.1017/S0022112094002909)
- Yeo, K. S., Zhao, H. Z. & Khoo, B. C. 2001 Turbulent boundary layer over a compliant surface: absolute and convective instabilities. *J. Fluid Mech.* **449**, 141–168. (doi:10.1017/S0022112001006206)
- Yurchenko, N. F. & Babenko, V. V. 1987 Stability criterion of three-dimensional perturbations on concave elastic surfaces. *J. Eng. Phys. Thermophys.* **52**, 568–573. (doi:10.1007/BF00873311)